

Article

Cobalt-Based Metal-Organic Framework Nanoparticles with Peroxidase-like Catalytic Activity for Sensitive Colorimetric Detection of Phosphate

Zhichen Deng ¹, Huifeng Zhang ¹, Ping Yuan ¹, Zhengquan Su ² , Yan Bai ¹, Zhina Yin ^{1,*} and Jincan He ^{1,*}

¹ Guangdong Engineering Research Center of Public Health Detection and Assessment, Guangdong Pharmaceutical University, Guangzhou 510310, China; ggjottodeng@163.com (Z.D.); 13715060054@163.com (H.Z.); y18883851784@163.com (P.Y.); angell_bai@163.com (Y.B.)

² Guangdong Engineering Research Center of Natural Products and New Drugs, Guangdong Provincial University Engineering Technology Research Center of Natural Products and Drugs, Guangdong Pharmaceutical University, Guangzhou 510006, China; suzhq@scnu.edu.cn

* Correspondence: yinzhina@gdpu.edu.cn (Z.Y.); hejincan@gdpu.edu.cn (J.H.); Tel.: +86-20-34055161 (J.H.); Fax: +86-20-34055355 (J.H.)



Citation: Deng, Z.; Zhang, H.; Yuan, P.; Su, Z.; Bai, Y.; Yin, Z.; He, J. Cobalt-Based Metal-Organic Framework Nanoparticles with Peroxidase-like Catalytic Activity for Sensitive Colorimetric Detection of Phosphate. *Catalysts* **2022**, *12*, 679. <https://doi.org/10.3390/catal12070679>

Academic Editors: Bernadette-Emőke Teleky, Dan Cristian Vodnar, Laura Mitrea, Lavinia Calinoiu, Szabo Katalin and Bianca-Eugenia Ștefănescu

Received: 16 May 2022

Accepted: 20 June 2022

Published: 22 June 2022

Publisher's Note: MDPI stays neutral with regard to jurisdictional claims in published maps and institutional affiliations.



Copyright: © 2022 by the authors. Licensee MDPI, Basel, Switzerland. This article is an open access article distributed under the terms and conditions of the Creative Commons Attribution (CC BY) license (<https://creativecommons.org/licenses/by/4.0/>).

Abstract: Appropriate addition of phosphate salt in food can improve the food quality and taste. However, extensive intake of phosphate salt may lead to some human diseases such as hyperphosphatemia and renal insufficiency. Thus, it is essential to establish a cost-effective, convenient, sensitive, and selective method for monitoring phosphate ion (Pi) to ensure food quality control. In this work, a Co-based metal-organic frameworks (Co-MOF) nanomaterial with dual functions (peroxidase-like activity and specific recognition) was designed for acting as a catalytic chromogenic platform for sensitive detection of Pi. The Co²⁺ nodes not only provide high enzyme-like activity to catalyze the 3,3',5,5'-tetramethylbenzidine (TMB) substrate to blue oxTMB (652 nm) but also act as selective sites for Pi recognition. The use of cationic organic ligands (2-methylimidazole) and cationic metal ions (Co²⁺) endows the Co-MOF with a strong positive surface charge, which is beneficial to the capture of negative-charged Pi and the dramatically suppressed TMB oxidation. When Pi exists, it specifically adsorbs onto the Co-MOF through the Co-O-P bond and the strong electrostatic interaction, leading to the change of surface charge on Co-MOF. The peroxidase-like catalytic activity of Co-MOF is thus restrained, causing a different catalytic effect on TMB oxidation from that without Pi. Based on this principle, a colorimetric assay was established for rapid and sensitive detection of Pi. A good linear relationship was obtained between Pi concentration and the absorbance at 652 nm, with a linear range of 0.009–0.144 mg/L and a detection limit of 5.4 µg/L. The proposed assay was applied to the determination of Pi in actual food samples with recoveries of 92.2–108% and relative standard deviations (RSDs) of 2.7–7.3%, illustrating the promising practicality for actual samples analysis.

Keywords: metal-organic framework; peroxidase-like catalytic activity; phosphate; colorimetric assay; food samples

1. Introduction

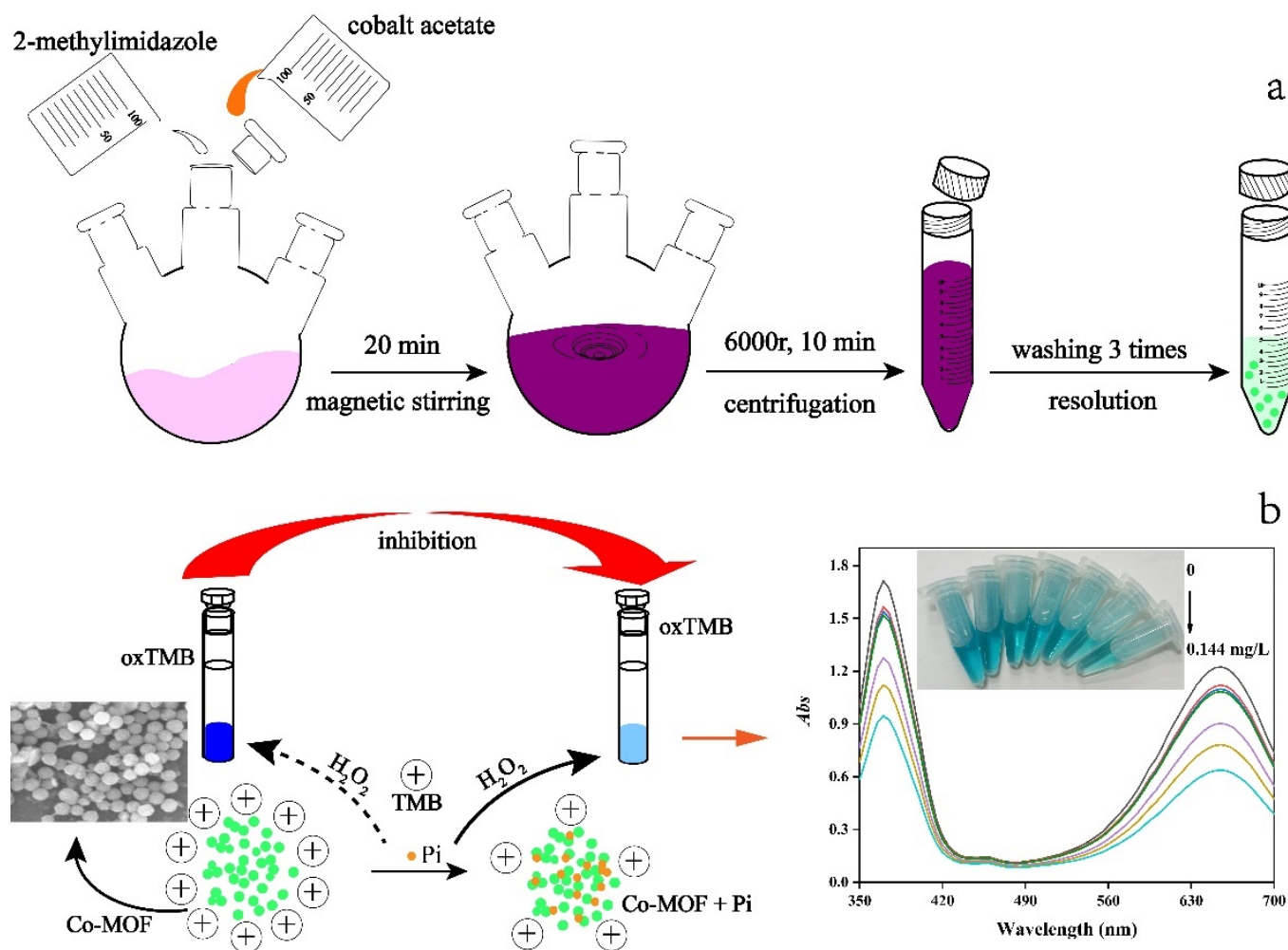
Phosphate salt is one of the most widely used food additives. It can be used for food processing to work as a water retention agent, quality improver, emulsion dispersant, and so on [1]. It plays an important role in improving food quality. However, excessive phosphate ion (Pi) not only causes superfluous water absorption and poor taste of the product, but also affects the human body's absorption of calcium, magnesium, iron, zinc, and other minerals, easily leading to health problems such as growth retardation, bone deformity, and osteoporosis. Therefore, it is essential to establish a cost-effective, convenient, sensitive, and selective method for the detection of Pi to ensure food safety.

Up to now, many analytic approaches have been developed for the detection of Pi, including the fluorescence method [2–5], chromatography [6,7], and electrochemical method [8–11]. However, these methods require precious instruments, which are not practical for on-site and large-scale analysis. The colorimetric method [12–15] is an analytical method based on the color depth of the tested solution. It attracts increasing attention due to the advantages of no need for the complex instrument, easy operation, quick response, and adaptable sensitivity.

In recent years, nanomaterials with intrinsic mimic enzyme activity have been drawing intensive interest for colorimetric assay [16–18]. Compared to natural enzymes, nanoenzymes show unique superiorities in low cost, simple synthesis, good stability, and good resistance to harsh conditions [19]. Metal-organic framework (MOF) nanomaterials formed by metal ions and organic ligands are promising nanoenzymes due to their versatile nature: (1) the rich metal nodes in MOF allow them to selectively recognize certain species through specific interactions, and the porosity can facilitate mass transport to promote the recognition process rapidly, both of which provide the foundation for the selective and fast detection of targets; (2) either metal nodes or organic ligands can be adjusted to achieve multifunctional activity; (3) several paramagnetic metal nodes-based MOFs have recently been found to exhibit catalytic activity to trigger a chromogenic reaction. So the MOF integrating recognition ability, porous structure, and catalytic activity all-in-one provide a favorable catalytic platform for high-performance colorimetric sensing of an analyte.

For Pi detection, Li X. et al. [20] proposed a dual-channel ratiometric colorimetric sensing of Pi based on the analyte-triggered differential oxidase-mimicking activity changes of oxidized UiO-66(Ce/Zr). The method shows high selectivity originating from the recognition of Zr⁴⁺ sites to Pi, however, the introduction of two chromogenic reactions is complicated and needs more time to operate. This group also proposed an enhanced Pi detection method, which used Zr(IV) ions to synergistically inhibit the peroxidase-like catalytic activity of hydrophilic Fe₃O₄ nanocubes [14]. The Zr(IV) ions worked as a mediator to promote the reaction kinetics and enhance the specificity of the recognition process so that the analytic performance was improved. However, the addition of the Zr(IV) ions mediator not only complicates the analytical procedure, but also brings an external factor that may influence the detection, neither of which is desirable in actual analysis. Combining the mediator with the nanoenzyme material to construct an integrated platform is generally convenient and welcome.

Taking the above aspects into consideration, a colorimetric method based on the target-induced peroxidase-like activity changes of Co-MOF is proposed for rapid, sensitive, and selective detection of Pi (Scheme 1). The Co²⁺ nodes not only provide good peroxidase-like activity to catalyze the 3,3',5,5'-tetramethylbenzidine (TMB) substrate to blue oxTMB (652 nm), but also acts as specific sites for Pi recognition. The use of cationic ligand (2-methylimidazole) and cationic metal ligand (Co²⁺) endows the MOF material with a strong positive surface charge, which is beneficial to the capture of Pi and the suppressed TMB oxidation. When Pi exists, it specifically adsorbs onto the Co-MOF through Co-O-P bond and strong electrostatic interaction. Accordingly, the surface charge of Co-MOF changes, leading to the different catalytic effects on the TMB substrates in comparison to that without the addition of Pi. Based on this principle, a catalytic colorimetric assay for rapid, sensitive, and selective detection of Pi was realized.



Scheme 1. Diagram for synthesis process of Co-MOF (a), and colorimetric sensing of Pi based on the target-induced differential peroxidase-like activity changes of Co-MOF (b).

2. Results and Discussion

2.1. Preparation and Characterization of Co-MOF

As illustrated in Scheme 1a, the Co-MOF is prepared with a one-pot co-precipitation method [21] using cobalt acetate and 2-methylimidazole. The Co^{2+} nodes provide active sites for peroxidase-like catalytic activity and specific binding to Pi. The cationic 2-methylimidazole cooperating with cationic Co^{2+} facilitates the formation of Co-MOF with a strong positive surface charge. To obtain superior catalytic activity, six kinds of Co-MOF nanomaterials were prepared with different 2-methylimidazole/cobalt ion salt mole ratios (10:10, 80:10, 160:10, 240:10, 320:10, 640:10). The catalytic activity of these six Co-MOF nanomaterials was investigated for catalytic oxidation of TMB in the presence of H_2O_2 . As displayed in Figure S1, the Co-MOF (320:10)-involved catalytic system exhibits the highest absorbance at 652 nm. The scanning electron microscopy (SEM) images of three Co-MOF nanomaterials (240:10, 320:10, 640:10) were collected. Two kinds of Co-MOF nanomaterials (240:10, 640:10) show layered hexagon (Figure S2a,b), while the Co-MOF (320:10) exhibits a regular spherical morphology with an average diameter of 145 nm (Figure 1). Considering the catalytic activity, the Co-MOF (320:10) was selected for further characterization and experiments.

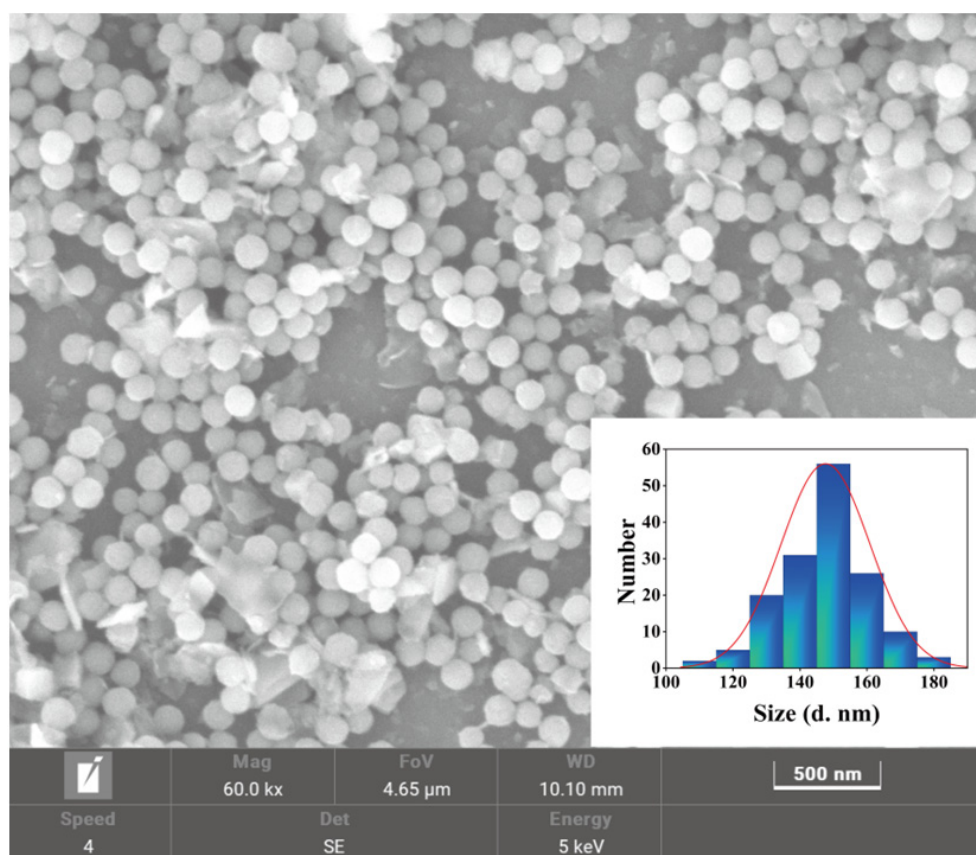


Figure 1. The SEM image and the size distribution (inserted).

The sharp peaks in X-ray diffractometry (XRD) spectrum (Figure 2a) at 7.5° (110), 11.7° (220), 18.5° (321), 32.1° (235), 38.5° (110), 51.3° (024), 58.0° (031) show the crystalline nature of Co-MOF. As depicted in Figure 2b, there is a weight loss appearing in the ranges of 70 – 132°C in the thermogravimetric (TG) curve, which is probably caused by water evaporation in the Co-MOF. As the temperature rises to 216°C , another weightlessness occurs possibly attributing to the loss of coordinated water molecules. Subsequently, the weightlessness of 216 – 510°C generates mainly due to the exfoliation of organic ligands. When the temperature is higher than 510°C , the structure of Co-MOF begins to crumble and the metal oxide is formed. It illustrates the good thermal stability of Co-MOF. The Fourier transform infrared (FT-IR) spectrum for functional groups in Co-MOF is exhibited in Figure 2c. The absorption peak at 419 cm^{-1} belongs to the flexural vibration of Co-N. The symmetric vibration of COO^- leads to an absorption bond at 1355 cm^{-1} . The feature absorption peaks at 3392 cm^{-1} and 3631 cm^{-1} correspond to vibrative traction of N-H in Co-MOF. The constitution of Co-MOF was demonstrated by X-ray photoelectron spectroscopy (XPS). As exhibited in Figure 2d, peaks of Co2p, C1s, O1s, and N1s exist in the XPS diagram, confirming the existence of Co, C, O, and N in the Co-MOF. Figure S3 displays XPS spectra deconvolution of Co2p of Co-MOF. There are four matched curve peaks in the spectrum. The modules at 781.3 eV and 797.2 eV correspond to cobalt of the Co-N bond, while the modules at 786.9 eV and 802.9 eV are assigned to the Co-O bond. The energy dispersive spectrometry (EDS) curve (Figure S4a) further confirms the existence of Co, C, O, and N with the wt% of 69.3, 17.5, 10.7, 2.5 for these four elements, respectively.

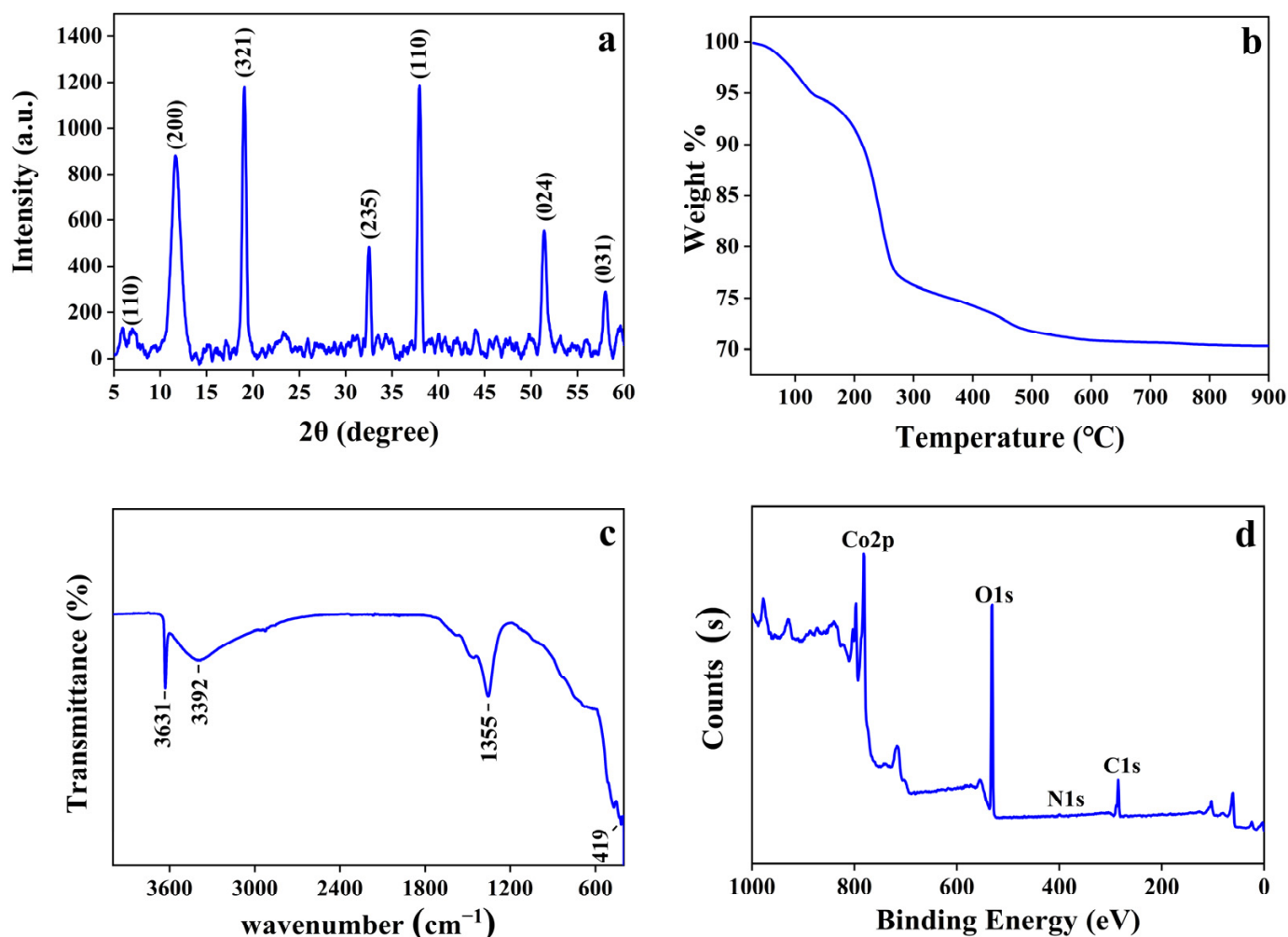


Figure 2. The XRD pattern (a), TG curve (b), FTIR spectrum (c), and XPS diagram (d) of Co-MOF.

The nitrogen adsorption-desorption isotherms of Co-MOF exhibit a type II curve (Figure S4b). The specific surface is $53.62 \text{ m}^2/\text{g}$, with a total pore volume of $0.1761 \text{ cm}^3/\text{g}$ and an average pore size of 13.14 nm (Table S1). The large specific surface and porosity structure provide adequate contact conditions for Co-MOF and catalytic chromogenic substrate. Moreover, the Co^{2+} nodes can not only provide good peroxidase-like activity to catalyze the TMB substrate to blue oxTMB, but also act as selective sites for Pi recognition. Therefore, the porosity structure and special composition enable Co-MOF to be a high-performance catalytic chromogenic platform for the detection of Pi.

2.2. Peroxidase-like Activity of Co-MOF

Firstly, TMB was used as a chromogenic substrate to investigate the peroxidase-like property of Co-MOF in the presence of H_2O_2 . As shown in Figure 3, either TMB or Co-MOF is colorless, while the system of Co-MOF + TMB + H_2O_2 turns blue and causes a strong absorption peak at 652 nm . Similar to the TMB case, the Co-MOF can also catalyze the chromogenic reaction of ABTS and OPD in the presence of H_2O_2 , exhibiting typical peroxidase-like catalytic activity.

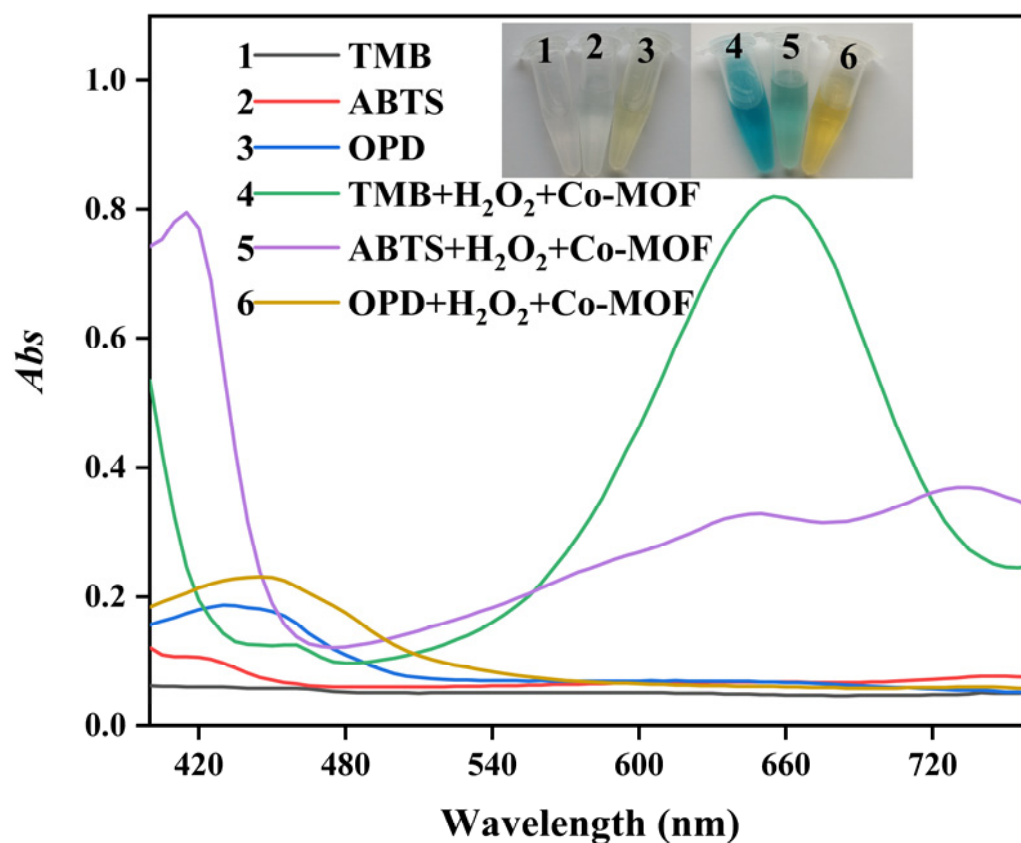


Figure 3. The absorption spectra and corresponding color change for catalytic oxidizing three substrates (TMB, ABTS, OPD) using Co-MOF as a catalyst.

The steady-state kinetic analysis of Co-MOF was carried out to gain more details on the peroxidase-like property. The kinetic data were obtained by changing either the concentration of H_2O_2 or TMB. As shown in Figure 4, the concentration of substrate plays a great role in the catalytic activity of Co-MOF, displaying the typical Michaelis-Menten behavior. The important kinetic parameters (K_m and V_{max}) are listed in Table S2. K_m is a key parameter expressing the affinity of an enzyme to a substrate. It is noticed that a lower K_m value implies a stronger affinity between the enzyme and the substrate [22]. Compared with horseradish peroxidase (HRP), the Co-MOF displays no superiority on K_m and V_{max} for TMB and H_2O_2 . However, the Co-MOF with low cost is more easy to prepare and preserve in comparison to HRP. Compared to (MIL-53(Fe) [23] and Fe-Co alloy NPs [24], the Co-MOF exhibits comparable or even weaker affinity toward H_2O_2 . The results are not so satisfactory. But it is notable that the K_m value of the Co-MOF for TMB is the lowest among the mentioned nanomaterials (MIL-53(Fe) and Fe-Co alloy NPs), indicating the high affinity to TMB and less requirement of TMB for the catalytic reaction. The good affinity is probably attributed to Co^{2+} nodes, the large specific surface, and porosity structure of Co-MOF. The Co^{2+} nodes provide good enzyme-like activity to catalyze the TMB substrate to blue oxTMB. Besides, the large specific surface and porosity structure provide space for sufficient contact of Co-MOF and catalytic substrate.

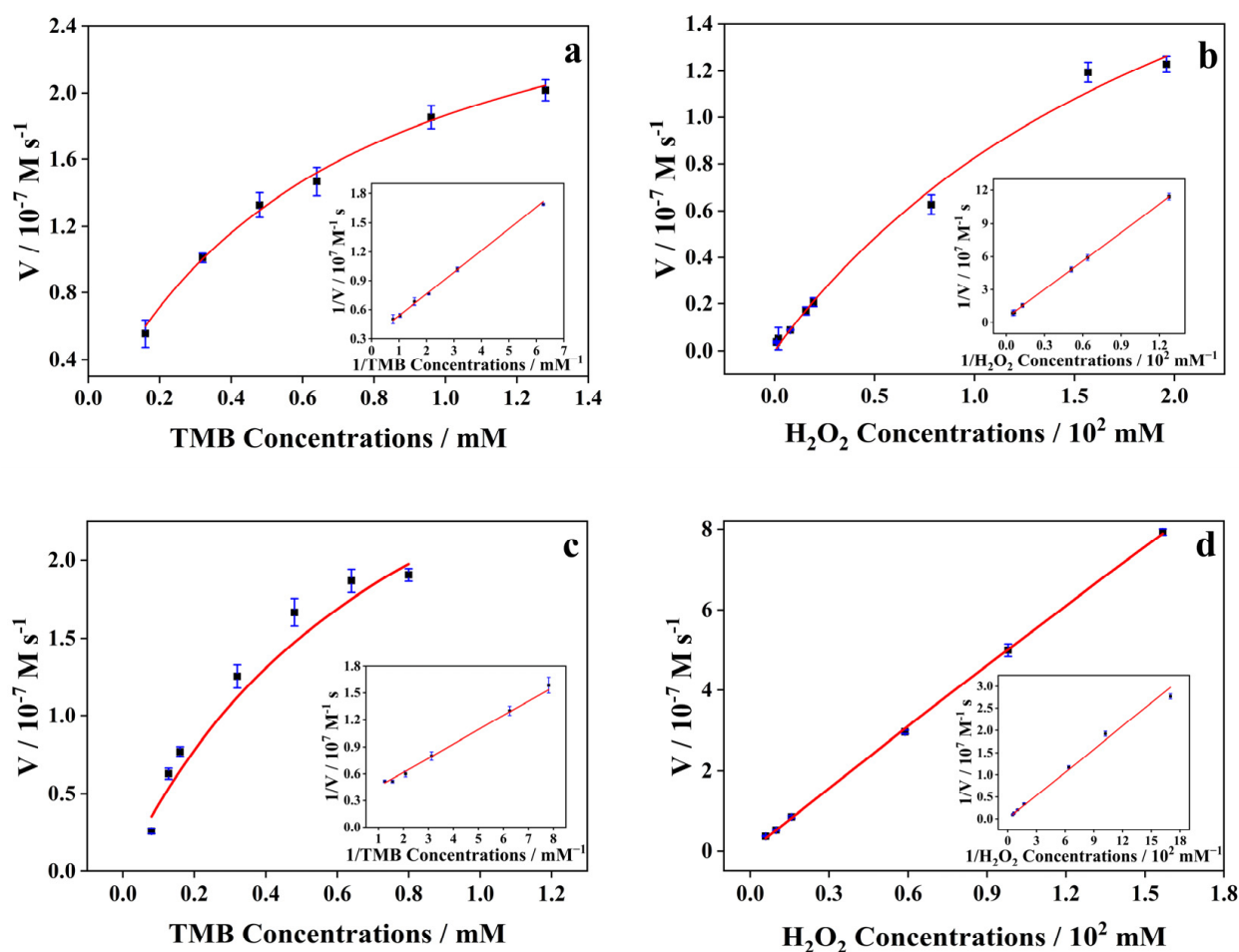


Figure 4. Michaelis-Menten pattern and Lineweaver-Burk pattern (insets) for steady-state dynamics study in Co-MOF and HRP by altering the concentration of TMB with a constant concentration of H_2O_2 (a,c), and altering the concentration of H_2O_2 with a constant concentration of TMB (b,d). Three parallel sets were measured at the same time.

In order to confirm the active sites for catalysis of Co-MOF, a series of cobalt ions, 2-methylimidazole, and Co-MOF with different concentrations were applied to catalytic chromogenic reaction using TMB as substrate. As shown in Figure S5a, the absorbance at 652 nm in the 2-methylimidazole-involved catalytic system shows little change with the increase of 2-methylimidazole concentration. The absorbance of the cobalt ions-involved catalytic system enhances slowly, while the Co-MOF-involved catalytic system increased remarkably. This phenomenon demonstrates the Co^{2+} nodes play the main role in catalytic performance of Co-MOF. Significantly, the absorbance of the Co-MOF-involved catalytic system is much higher than that of cobalt ions at the same concentration. It is possible due to that the large specific surface and porosity structure of Co-MOF provide sites for gathering H_2O_2 and TMB, thus improving the catalytic efficiency greatly.

It is of great importance to ascertain whether the observed peroxidase-like activity resulted from the lixiviation of cobalt ions or Co-MOF itself. The Co-MOF was incubated in HAc-NaAc buffer (pH 4.5) at room temperature (25°C) for 5 min. The supernatant was then obtained by centrifugation and used for catalytic oxidation of TMB in the presence of H_2O_2 . As displayed in Figure S5a, the Co-MOF involved catalytic system exhibits increasing absorbance at 652 nm along the time, nevertheless, the lixiviation solution involved in catalytic system shows almost invariable absorbance at 652 nm. It demonstrates that the peroxidase-like activity originates from the Co-MOF itself rather than the lixiviation solution.

2.3. Inhibition of Pi on Co-MOF Catalyzed System

As previously reported in the literature, various metal species [25–27] (including Co) can adsorb Pi via strong interactions. Since there are both peroxidase-like active sites and Pi specific sites existing in Co-MOF, the peroxidase-like catalytic activity of the prepared material is likely to be impacted by the addition of Pi. To test this hypothesis, the Co-MOF was employed for catalyzing TMB reactions in the presence/absence of Pi. As presented in Figure 5, the TMB, Co-MOF, and TMB + H₂O₂ system (curves 1, 2, 3) show hardly any characteristic absorption peaks and color changes. The TMB + Co-MOF system (curve 4) exhibits a weak absorption peak at 652 nm and the color turns to light blue, illustrating an oxidase-like activity of Co-MOF [28]. The absorbance in the catalytic system of Co-MOF + TMB + H₂O₂ + Pi (curve 6) is obviously lower than that in the system of Co-MOF + TMB + H₂O₂ (curve 5). This phenomenon reveals the suppressed TMB oxidation of Co-MOF with the existence of Pi. After combining with Pi, the active sites in Co-MOF for peroxidase activity were masked, which hindered the oxidation of TMB to oxTMB. In addition, the specific adsorption of Pi also blocked the pores of Co-MOF, which made it difficult for the substrate to diffuse the active sites. Therefore, the peroxidase-like activity of Co-MOF was obviously hindered in the presence of Pi.

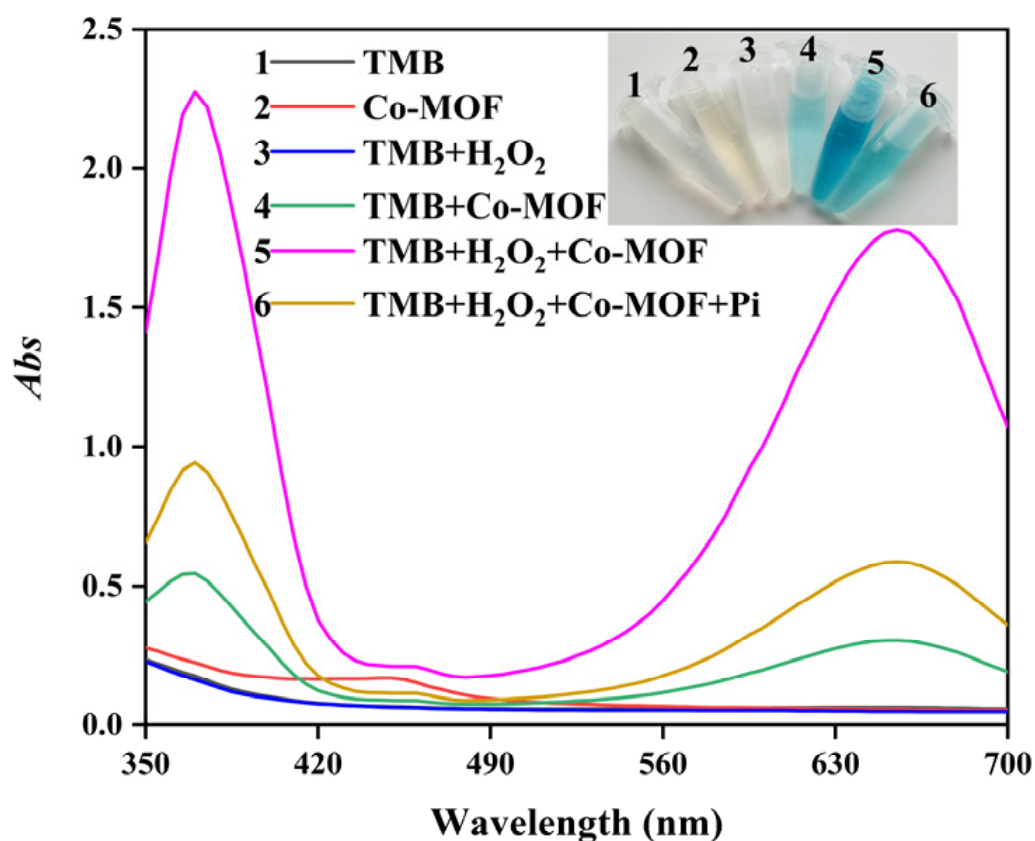


Figure 5. The absorption spectra and corresponding color change of diverse catalytic reaction systems.

The catalytic conditions (e.g., pH, reaction temperature, reaction time, and substrate concentration) for possible influencing the catalytic activity of Co-MOF were investigated in the presence/absence of Pi. Figure S6a,b display that Co-MOF exhibits the highest catalytic activity at pH 4.5 and 25 °C. TMB and H₂O₂ also play a great role in catalytic activity. It illustrates that the highest catalytic activity reaches with the conditions of 3 mmol/L TMB concentration, 0.80 mL TMB adding volume, and 0.80 mL H₂O₂ (Figures S6c,d and S7a). The catalytic activity increases with the concentration of Co-MOF. The greatest absorbance difference achieves with a Co-MOF concentration of 1.8 mg/L (Figure S7b). The absorbance of the system at 652 nm also varies with reaction time (Figure S7c). The absorbance increases

with the reaction time in 5–40 min and starts to slow down slightly after 40 min. In fact, 15 min is enough to obtain a suitable absorbance.

The catalytic stability of Co-MOF with different storage days was also evaluated. A batch of Co-MOF was prepared and stored in a dryer. A certain amount of Co-MOF was taken out from the dryer every day for the catalytic oxidation of TMB. The absorbance of the catalytic reaction was recorded every day for different storage days under the optimal catalytic conditions. As shown in Figure S7d, the Co-MOF exhibits a stable catalytic activity in 16 days either in the absence or in the presence of Pi, with the relative standard deviation (RSD) less than 10%. It illustrates that the Co-MOF exhibits good stability with storage time.

To further understand the mechanism of Pi inhibiting Cu-MOF catalytic activity, several characterizations were conducted including FTIR, XPS, zeta potential, and electron spin resonance (ESR) measurement. As demonstrated in Figure S8a, the addition of Pi into Co-MOF causes a remarkable FTIR absorption peak at 1010 cm^{-1} , which should be assigned to the P-O bond [2,29]. The high-resolution XPS pattern (Figure S8b) verifies the existence of Pi in Co-MOF after the addition of Pi. The binding energy of Co 2p changes from 781.5 eV to 780.9 eV, and from 797.4 eV to 797 eV, while the binding energy of O 1s changes from 531.6 eV to 531.1 eV (Figure S7c,d), both of which indicate the interaction of Co, O atoms in Co-MOF with Pi and the formation of Co-O-P bond. The zeta-potential value of Co-MOF in the absence/presence of Pi was measured (Figure S9). The zeta potential value of bare Co-MOF is +20.93 mV, while it decreases to +13.83 mV after the addition of Pi, probably due to the interaction between Co-MOF and Pi. The ESR spectra of Co-MOF were also measured using 5,5-dimethyl-1-pyrroline *N*-oxide (DMPO) as a probe for $\cdot\text{OH}$ radicals (Figure S10). It illustrates that the Co-MOF can catalyze H_2O_2 to generate $\cdot\text{OH}$, clearly demonstrating the peroxidase-like activity of the nanomaterial [25]. After the addition of Pi, less $\cdot\text{OH}$ can be observed, which may be attributed to the inhibition of Pi on the catalytic activity.

2.4. Colorimetric Assay for Detection of Pi

Based on the inhibition of Pi to the peroxidase-like catalytic activity of Co-MOF, a colorimetric assay was established for Pi detection. As shown in Figure 6, under the optimized catalytic conditions, the addition of Pi to the Co-MOF inhibits the catalytic oxidation of TMB. The absorbance at 652 nm decreases gradually as the increase of Pi concentration. A good linear range was obtained from 0.009 to 0.144 mg/L with a correlative coefficient (r) of 0.9931. The limit of detection (LOD) was calculated to be $5.4\text{ }\mu\text{g/L}$ according to three times the signal-to-noise ($S/N = 3$) ratio. The analytic performance of the proposed method with other nanomaterials-related methods for Pi detection was compared [10,30–35] (Table S3). It exhibits that the LOD of the proposed method is the lowest among the colorimetric method [33–35], and even lower than some fluorescence methods [30,31] and voltammetry [10]. The low LOD is probably due to the special structure and composition of Co-MOF. Different from common MOFs coordinated by cationic metal ions and anionic organic ligands, the proposed Co-MOF is coordinated by cationic metal ions (Co^{2+}) and cationic ligands (2-methylimidazole). The dual cationic components of Co-MOF endow it with a strong positive surface charge (+20.93 mV), which is beneficial to the capture of Pi and the dramatically suppressed TMB oxidation. So the low LOD for Pi detection can be realized. Furthermore, the proposed Co-MOF was prepared by a one-pot method of 20 min without the use of toxic organic solvents, exhibiting the synthetic superiorities over other nanomaterials and natural enzymes with a complicated procedure.

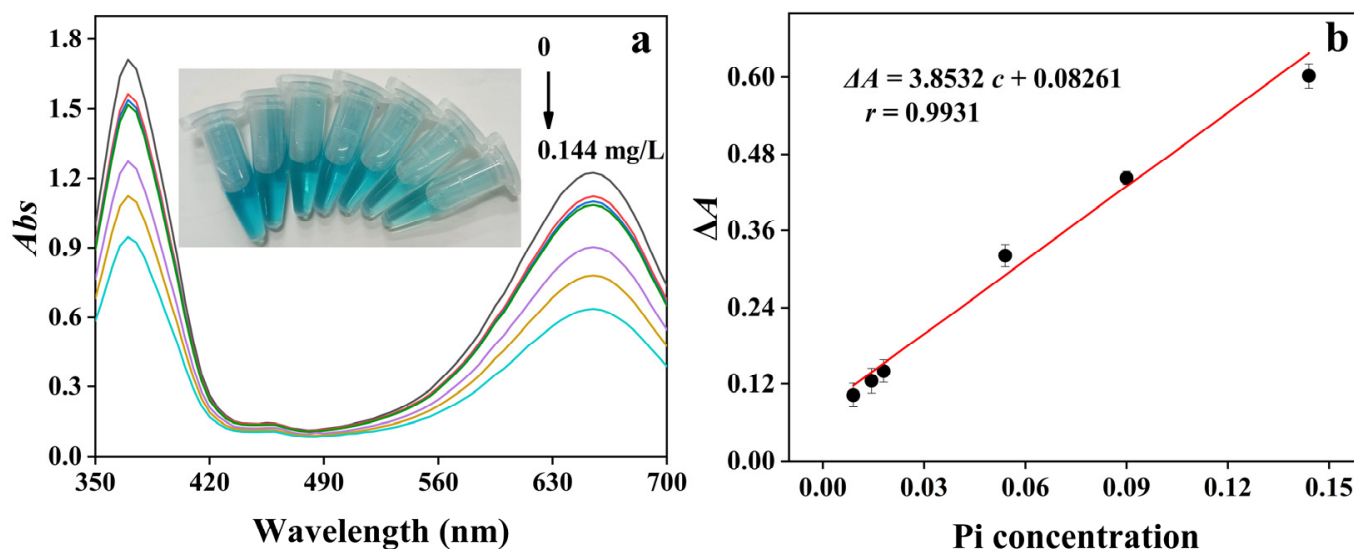


Figure 6. The absorption spectra and visual color changes (a), and the linear fitting curve between the Pi concentration and the absorbance difference (b). $\Delta A = A_0 - A_1$, where A_0 and A_1 represent the absorbance in the system of Co-MOF/TMB- H_2O_2 system without and with the addition of Pi, respectively. The wavelength of absorbance was 652 nm. Error bars were obtained from three parallel tests.

2.5. Selectivity

The selectivity of the method was investigated by monitoring the absorbance change at 652 nm after adding a different substance into the system of Co-MOF + Pi + TMB + H_2O_2 . As depicted in Table 1, Most inorganic anions, intermediate inorganic cations, and amino acids show negligible effect with a relative error of less than $\pm 8\%$, indicating the good selectivity of the colorimetric assay.

Table 1. Tolerance ratio of different co-existing substances for determination of 0.1 mg/L Pi.

Coexistent Ions	Tolerance Ratio	Relative Error (%)	Coexistent Ions	Tolerance Ratio	Relative Error (%)
Na ⁺	400	−5.8	Al ³⁺	50	−6.9
Mg ²⁺	50	−6.7	CH ₃ COO [−]	700	−5.4
Cu ²⁺	50	3.8	F [−]	250	−4.1
Zn ²⁺	100	−7.4	arginine	80	7.7
Fe ³⁺	100	7.6	glutamate	60	0.5
SO ₄ ^{2−}	100	−5.4	aspartate	20	4.1
CO ₃ ^{2−}	200	−3.2	cysteine	50	−4.3
HCO ₃ [−]	200	−4.0	glycine	40	−6.6
K ⁺	200	4.7	glucose	50	−5.9

2.6. Determination of Pi in Actual Samples

To evaluate the practicability, the colorimetric assay was applied to the determination of Pi in actual samples such as bottled drinking water, biscuits, and milk. As displayed in Table 2, the Pi content is 3.38 ± 0.17 g/kg and 0.69 ± 0.02 g/L in biscuits and milk samples, respectively. While no Pi has been detected in bottled drinking water. The results agree with that of the Chinese National standard method [36] ($p > 0.05$). The recoveries are 92.2–108% and RSDs are 2.7–7.3%, illustrating the accuracy of the method and its applicability in complex samples.

Table 2. Determination of Pi in actual food samples with the proposed method.

Sample	Added (g/kg)/(g/L)	Detcted (g/kg)/(g/L)	Recovery (%)	RSD ($n = 3$, %)	Standard Method [36] (g/kg)/(g/L)	<i>t</i> -Test
Biscuits	0	3.83 ± 0.14	-	-	3.38 ± 0.17	$p = 0.083 > 0.05$
	0.5	4.35 ± 0.038	103.8	7.3	-	-
	2	5.97 ± 0.20	107.4	6.8	-	-
Milk	0	0.73 ± 0.025	-	-	0.69 ± 0.02	$p = 0.097 > 0.05$
	0.025	0.96 ± 0.019	92.2	5.4	-	-
	1	1.71 ± 0.026	98.0	2.7	-	-
Drinking water	0	ND	-	-	ND	-
	0.009	0.0097 ± 0.00068	107.8	7.1	-	-
	0.036	0.033 ± 0.00094	92.6	2.8	-	-

3. Experimental Part

3.1. Chemical and Materials

Cobalt acetate, 2-methylimidazole, acetate acid, sodium acetate anhydrous, HRP, TMB, ABTS, and OPD were obtained from Shanghai Aladdin Biochemical Technology Co., Ltd. (Shanghai, China). Hydrogen peroxide (H₂O₂, 30 wt%) was purchased from Guangzhou Chemical Reagent Factory (Guangzhou, China). All chemical reagents were at least analytical pure and used without further purification. Ultrapure water (>18.2 MΩ·cm) was produced from an ultrapure water treatment system and used throughout the experiments.

3.2. Apparatus

FT-IR spectrum was collected on a Nicolet iS10 infrared spectrometer (Thermo Fisher Scientific, Waltham, MA, USA). The SEM photographs were observed from scanning electron microscopy (SEM, Zeiss Sigma 500, Oberkochen, Germany). XRD analysis was performed on a Bruker D8 Advance diffractometer (Bruker, Berlin, Germany). The TG data was collected on a TG analyzer (DSC200F3, Netzsch, Selb, Germany) at a rate of 30 °C/10 min in a range of 30–900 °C. Elemental analysis was performed on an AXIS SUPRA XPS instrument (Shimadzu, Kyoto, Japan). The TG analysis was carried out on a TGA/DSC1 TG analyzer (METTLER TOLEDO, Greifensee, Switzerland). The nitrogen adsorption desorption isotherms were measured on the ASAP 2020 PLUS HD88 instrument (Micromeritics, Norcross, GA, USA). The ESR spectrum was recorded on a Bruker E580 electron paramagnetic resonance spectrometer (Bruker, Berlin, Germany). The absorption spectra were obtained from a UV-3010 ultraviolet spectrophotometer (Hitachi, Tokyo, Japan). The absorbance was collected on a microplate reader (Bio-Rad Laboratories Instruments Company, Hercules, CA, USA).

3.3. Synthesis of Co-MOF

Co-MOF was synthesized using cobalt acetate and 2-methylimidazole through a one-pot co-precipitation method in ultrapure water according to a previous report [21] with minor modification. In detail, a series of various amounts of 2-methylimidazole were respectively dissolved in 100 mL ultrapure water to prepare six different concentrations of 2-methylimidazole aqueous solution (10 mmol/L, 80 mmol/L, 160 mmol/L, 240 mmol/L, 320 mmol/L, 640 mmol/L). The 10 mmol/L cobalt acetate aqueous solution was prepared in the same way as 2-methylimidazole. A series of 100 mL of 2-methylimidazole aqueous solution with six different concentrations and a 100 mL of 10 mmol/L cobalt acetate aqueous solution were mixed in a flask through magnetic stirring for 20 min at room temperature. The products were centrifugated at 6000 rpm for 10 min, followed by washing with ultrapure water three times to elute the unreacted metal ions and organic ligands. Six kinds of Co-MOF with different 2-methylimidazole/cobalt ion molar ratios were finally obtained by freeze-drying overnight.

3.4. Study of Catalytic Activity

The peroxidase-like catalytic activity of Co-MOF was studied by employing TMB, ABTS, and OPD as substrates, respectively. For a typical reaction system, 100 μL of 5.0 mmol/L TMB (or ABTS, OPD), 20 μL of H_2O_2 , and 200 μL of Co-MOF were added into a 20 mmol/L HAc-NaAc buffer (pH 4.5) with a final buffer volume of 2.0 mL. The absorption spectra of the mixture after reaction for 5 min were recorded by an ultraviolet spectrophotometer.

Kinetic measurements were performed using TMB as a substrate on a microplate reader at the absorption wavelength of 652 nm. The values of the kinetic constants were calculated based on the Lineweaver-Burk plots and the Michaelis-Menten equation of $v = V_{\max}[\text{S}]/(K_m + [\text{S}])$, where v was the initial rate, V_{\max} was the maximum reaction rate, $[\text{S}]$ was the concentration of the substrate, and K_m was the Michaelis constant.

3.5. Analytical Procedures

A series of 1.0 mL of Pi solution with different concentrations and 1.0 mL of 0.18 mg/mL Co-MOF were successively added into a centrifuge tube with 1.0 mL acetic acid/sodium acetate buffer (HAc/NaAc, 20 mmol/L, pH 4.5). The mixture was shaken and stood for 2 min. Afterwards, 0.80 mL of 3.0 mmol/L TMB and 0.80 mL of 0.98 mol/L hydrogen peroxide were added to the previous mixture. HAc/NaAc buffer solution was finally added and filled to 5 mL, followed by incubation for 25 min at 25 $^{\circ}\text{C}$. The absorption spectra were recorded on the UV-Vis spectrophotometer.

3.6. Determination of Pi in Actual Samples

Biscuits, milk, and bottled drinking water were purchased from the local market. A 0.5 g of biscuits and 1.0 mL of milk were placed into digestion vessels, respectively. Then, 10.0 mL of nitric acid, 1.0 mL of perchloric acid, and 2.0 mL of sulfuric acid were added, respectively. The mixture was heated on an adjustable electric furnace under 210 $^{\circ}\text{C}$ for 0.5 h, 230 $^{\circ}\text{C}$ for 1 h, and 250 $^{\circ}\text{C}$ for 1 h progressively, until the digestion mixture became transparent or pale yellow. The final digestion solution was diluted for 500 folds, followed by passing through cation exchange resin and 0.22 μm filter membrane. As for drinking water, it only required pretreatment of cation exchange resin and a 0.22 μm filter membrane. Finally, the obtained sample solution was used for analysis as procedures in Section 3.5.

4. Conclusions

In summary, a colorimetric assay was established for rapid and sensitive detection of Pi based on the peroxidase-like activity of Co-MOF. The proposed Co-MOF exhibited high peroxidase-like activity to catalyze chromogenic reactions and good specificity to recognize Pi, so the detection of Pi with high sensitivity and good selectivity was obtained. The current work holds several advantages. (1) MOF integrating recognition ability, porous structure, and catalytic activity all-in-one provides a favorable catalytic platform for high-performance colorimetric sensing of an analyte. (2) The color change can be observed through the naked eye without the use of complicated apparatus, providing a convenient candidate for on-site and visual detection. (3) The LOD is quite advantageous, which is much lower than most methods. (4) The assay was applied to real samples with satisfactory results. Although some issues may still exist in the detection system (for instance, the difficulty for the reusability of Co-MOF in the sensing platform), the advantages of easy operation, fast response, ultra-high sensitivity, good selectivity, and favorable reliability will endow the method with great promise in the on-site inspection of food safety, environmental water monitoring, and other fields. It is also expected that with the combination of functional components, such as multi-metal, magnetic metal oxides, and recognition elements (aptamer, et al.), the Co-MOF can be extended to develop a various colorimetric assay for other analytes.

Supplementary Materials: The following supporting information can be downloaded at: <https://www.mdpi.com/article/10.3390/catal12070679/s1>, Figure S1: Co-MOF prepared with different 2-methylimidazole/cobalt salt mole ratio for catalytic oxidizing TMB in presence of H₂O₂. The absorbance was obtained at 652 nm; Figure S2: The SEM images of Co-MOF prepared with 2-methylimidazole/cobalt salt mole ratio of 240: 10 (a), and 640: 10 (b); Figure S3: The XPS spectra of Co-MOF for Co 2p; Figure S4: The EDS spectrum (a) and nitrogen adsorption and desorption isotherms (b) of Co-MOF; Figure S5: The absorbance changes of TMB-H₂O₂ system catalyzed with different concentrations of substance (a). Time dependent absorbance change of Co-MOF and leaching solution-involved TMB-H₂O₂ catalytic system (b). The absorbance was measured at 652 nm; Figure S6: The conditions of reaction pH (a), reaction temperature (b), TMB concentration (c), TMB adding volume (d) on the catalytic activity of Co-MOF; Figure S7: The conditions of H₂O₂ volume (a), Co-MOF concentration (b), time (c) on the catalytic activity of Co-MOF, and the catalytic stability of Co-MOF for 16 storage days (d); Figure S8: The FT-IR spectra of Co-MOF after addition of Pi (a), the XPS pattern of Co-MOF after addition of Pi (b), the XPS pattern of Co 2p in Co-MOF with and without Pi addition (c), and the XPS pattern of O 1s in Co-MOF with and without Pi addition (d); Figure S9: Zeta potential value of Co-MOF with and without the addition of Pi; Figure S10: The ESR spectra of Co-MOF before and after adding Pi. (25 mM DMPO was added.); Table S1: The BET parameters of Co-MOF; Table S2: Comparison of the apparent Michaelis-Menten constant (K_m), maximum reaction rate (V_{max}) of Co-MOF with other reported substance or nanomaterials; Table S3: Comparison of the proposed method with other nanomaterials-related methods for Pi determination.

Author Contributions: Conceptualization, Z.D. and J.H.; methodology, Z.Y.; software, Z.D.; validation, Z.D., H.Z. and J.H.; formal analysis, Z.D.; investigation, Z.Y.; resources, J.H.; data curation, Z.D. and P.Y.; writing—original draft preparation, Z.D.; writing—review and editing, J.H.; visualization, Z.S.; supervision, J.H. and Y.B.; project administration, J.H. All authors have read and agreed to the published version of the manuscript.

Funding: This research was funded by National Natural Science Foundation of China (NO. 21804025), Science and Technology Planning Project of Xizang (Tibet) Autonomous Region of China (NO. XZ202001ZY0058G), Special Fund for “Climbing Plan” of Science and Technology Innovation Cultivation for Guangdong University Students in 2022 of China (NO. pdjh2022b0266), Science and Technology Program of Guangzhou, China (NO. 202103000089), Project for Innovation and Strong School of Department of Education of Guangdong Province, China (NO. 2019GCZX012) and Guangdong Demonstration Base for Joint Cultivation of Postgraduates (2019).

Data Availability Statement: All the relevant data used in this study have been provided in the form of figures and tables in the published article, and all data provided in the present manuscript are available to whom it may concern.

Acknowledgments: The authors would like to thank the Jushang Scientific Research Service Platform (mall.jsceshi.cn) for providing SEM, EDS, ESR, TG, FTIR, XRD, XPS measurement.

Conflicts of Interest: The authors declare no conflict of interest.

References

1. Kalantar-Zadeh, K.; Gutekunst, L.; Mehrotra, R.; Kovcsdy, C.P.; Bross, R.; Shinaberger, C.S.; Noori, N.; Hirschberg, R.; Benner, D.; Nissenson, A.R.; et al. Understanding sources of dietary phosphorus in the treatment of patients with chronic kidney disease. *Clin. J. Am. Soc. Nephrol.* **2010**, *5*, 519–530. [[CrossRef](#)] [[PubMed](#)]
2. Li, X.; Liu, P.; Niu, X.H.; Ye, K.; Ni, L.; Du, D.; Pan, J.M.; Lin, Y.H. Tri-functional Fe-Zr bi-metal-organic frameworks enable high-performance phosphate ion ratiometric fluorescent detection. *Nanoscale* **2020**, *12*, 19383–19389. [[CrossRef](#)]
3. Dwivedi, S.K.; Gupta, R.C.; Srivastava, P.; Singh, P.; Koch, B.; Maiti, B.; Misra, A. Dual fluorophore containing efficient photoinduced electron transfer based molecular probe for selective detection of Cr³⁺ and Pi ions through fluorescence “turn-on-off” response in partial aqueous and biological medium: Live cell imaging and logic application. *Anal. Chem.* **2018**, *90*, 10974–10981. [[CrossRef](#)] [[PubMed](#)]
4. Chandra, R.P.; Mandal, S. Europium-based metal-organic framework as a dual luminescence sensor for the selective detection of the phosphate anion and Fe³⁺ ion in aqueous media. *Inorg. Chem.* **2018**, *57*, 11855–11858. [[CrossRef](#)]
5. Asha, K.S.; Bhattacharjee, R.; Mandal, S. Complete transmetalation in a metal-organic framework by metal ion metathesis in a single crystal for selective sensing of phosphate ions in aqueous media. *Angew. Chem. Int. Edit.* **2016**, *55*, 11528–11532. [[CrossRef](#)] [[PubMed](#)]

6. Yi, R.; Song, P.; Liu, X.; Maruo, M.; Ban, S. Differences in dissolved phosphate in shallow-lake waters as determined by spectrophotometry and ion chromatography. *Limnology* **2020**, *21*, 329–339. [[CrossRef](#)]
7. Iammarino, M.; Haouet, N.; Taranto, A.D.; Berardi, G.; Benedetti, F.; Bella, S.D.; Chiaravalle, A.E. The analytical determination of polyphosphates in food: A point-to-point comparison between direct ion chromatography and indirect photometry. *Food. Chem.* **2020**, *325*, 126937. [[CrossRef](#)] [[PubMed](#)]
8. Wei, H.; Pan, D.; Zhou, Z.W.; Han, H.T.; Zhu, R.L. On-site electrochemical determination of phosphate with high sensitivity and anti-interference ability in turbid coastal waters. *Ecotox. Environ. Safe.* **2021**, *221*, 112444. [[CrossRef](#)] [[PubMed](#)]
9. Kalayci, S. A New phosphate selective electrode and its application in some foods. *Int. J. Electrochem. Sci.* **2021**, *16*, 210949. [[CrossRef](#)]
10. Wu, T.; Xia, D.; Xu, J.; Ye, C.Z.; Zhang, D.; Deng, D.W.; Zhang, J.S. Sequential injection-square wave voltammetric sensor for phosphate detection in freshwater using silanized multi-walled carbon nanotubes and gold nanoparticles. *Microchem. J.* **2021**, *167*, 106311. [[CrossRef](#)]
11. Ding, Y.; Zhao, M.; Yu, J.; Zhang, X.M.; Li, Z.M.; Li, H. Using the interfacial barrier effects of p-n junction on electrochemistry for detection of phosphate. *Analyst* **2020**, *145*, 3217–3221. [[CrossRef](#)]
12. Li, X.; Liu, B.X.; Hu, Z.; Liu, P.; Ye, K.; Pan, J.M.; Niu, X.H. Smartphone-assisted off-on photometric determination of phosphate ion based on target-promoted peroxidase-mimetic activity of porous $\text{Ce}_x\text{Zr}_{1-x}\text{O}_2$ ($x \geq 0.5$) nanocomposites. *Environ. Res.* **2020**, *189*, 109921. [[CrossRef](#)]
13. Pinyorosphatum, C.; Rattanarat, P.; Chaiyo, S.; Siangproh, W.; Chailapakul, O. Colorimetric sensor for determination of phosphate ions using anti-aggregation of 2-mercaptoethanesulfonate-modified silver nanoplates and europium ions. *Sens. Actuat. B Chem.* **2019**, *290*, 226–232. [[CrossRef](#)]
14. Li, X.; Liu, B.; Ye, K.; Ni, L.; Xu, X.C.; Qiu, F.X.; Pan, J.M.; Niu, X.H. Highly sensitive and specific colorimetric detection of phosphate by using Zr (IV) to synergistically suppress the peroxidase-mimicking activity of hydrophilic Fe_3O_4 nanocubes. *Sens. Actuat. B Chem.* **2019**, *297*, 126822. [[CrossRef](#)]
15. Nagul, E.A.; McKelvie, I.D.; Kolev, S.D. The use of on-line UV photoreduction in the flow analysis determination of dissolved reactive phosphate in natural waters. *Talanta* **2015**, *133*, 155–161. [[CrossRef](#)] [[PubMed](#)]
16. Wu, J.J.X.; Wang, X.Y.; Wang, Q.; Lou, Z.P.; Li, S.R.; Zhu, Y.Y.; Qin, L.; Wei, H. Nanomaterials with enzyme-like characteristics (nanozymes): Next-generation artificial enzymes (II). *Chem. Soc. Rev.* **2019**, *48*, 1004–1076. [[CrossRef](#)] [[PubMed](#)]
17. Ahmad, R.; Shanahan, J.; Rinaldo, S.; Kissel, D.S.; Stone, K.L. Co-immobilization of an enzyme system on a metal-organic framework to produce a more effective biocatalyst. *Catalysts* **2020**, *10*, 499. [[CrossRef](#)]
18. Liang, M.M.; Yan, X.Y. Nanozymes: From new concepts, mechanisms, and standards to applications. *Acc. Chem. Res.* **2019**, *52*, 2190–2200. [[CrossRef](#)]
19. Li, X.; Zhou, H.; Qi, F.; Niu, X.H.; Xu, X.C.; Qiu, F.X.; He, Y.F.; Pan, J.M.; Ni, L. Three hidden talents in one framework: A terephthalic acid-coordinated cupric metal-organic framework with cascade cysteine oxidase- and peroxidase-mimicking activities and stimulus-responsive fluorescence for cysteine sensing. *J. Mater. Chem. B* **2018**, *6*, 6207–6211. [[CrossRef](#)]
20. Li, X.; Niu, X.; Liu, P.; Xu, X.C.; Du, D.; Lin, Y.H. High-performance dual-channel ratiometric colorimetric sensing of phosphate ion based on target-induced differential oxidase-like activity changes of Ce-Zr bimetal-organic frameworks. *Sens. Actuat. B Chem.* **2020**, *321*, 128546. [[CrossRef](#)]
21. Qiu, P.P.; Yuan, P.; Deng, Z.C.; Su, Z.Q.; Bai, Y.; He, J.C. One-pot facile synthesis of enzyme-encapsulated Zn/Co-infinite coordination polymer nanospheres as a biocatalytic cascade platform for colorimetric monitoring of bacteria viability. *Microchim. Acta* **2021**, *188*, 322. [[CrossRef](#)] [[PubMed](#)]
22. Wang, J.Y.; Li, W.Y.; Zheng, Y.Q. Colorimetric assay for sensitive detection of phosphate in water based on metal-organic framework nanospheres possessing catalytic activity. *New J. Chem.* **2020**, *44*, 19683–19689. [[CrossRef](#)]
23. Ai, L.H.; Li, L.L.; Zhang, C.H.; Fu, J.; Jiang, J. MIL-53(Fe): A metal-organic framework with intrinsic peroxidase-like catalytic activity for colorimetric biosensing. *Chem.—Eur. J.* **2013**, *19*, 15105–15108. [[CrossRef](#)] [[PubMed](#)]
24. Chen, Y.J.; Cao, H.Y.; Shi, W.B.; Liu, H.; Huang, Y.M. Fe-Co bimetallic alloy nanoparticles as a highly active peroxidase mimetic and its application in biosensing. *Chem. Commun.* **2013**, *49*, 5013. [[CrossRef](#)]
25. Tang, X.Q.; Zhang, Y.D.; Jiang, Z.W.; Wang, D.M.; Huang, C.Z. Fe_3O_4 and metal-organic framework MIL-101(Fe) composites catalyze luminol chemiluminescence for sensitively sensing hydrogen peroxide and glucose. *Talanta* **2018**, *179*, 43–50. [[CrossRef](#)]
26. Yang, J.; Dai, Y.; Zhu, X.Y.; Wang, Z.; Li, Y.S.; Zhuang, Q.X.; Shi, J.L.; Gu, J.L. Metal-organic frameworks with inherent recognition sites for selective phosphate sensing through their coordination-induced fluorescence enhancement effect. *J. Mater. Chem. A* **2015**, *3*, 7445–7452. [[CrossRef](#)]
27. Zhu, X.Y.; Li, B.; Yang, J.; Li, Y.S.; Zhao, W.R.; Shi, J.L.; Gu, J.L. Effective adsorption and enhanced removal of organophosphorus pesticides from aqueous solution by Zr-based MOFs of UiO-67. *ACS Appl. Mater. Inter.* **2015**, *7*, 223–231. [[CrossRef](#)]
28. Yang, H.G.; Yang, R.T.; Zhang, P.; Qin, Y.M.; Chen, T.; Ye, F.G. A bimetallic (Co/2Fe) metal-organic framework with oxidase and peroxidase mimicking activity for colorimetric detection of hydrogen peroxide. *Microchim. Acta* **2017**, *184*, 4629–4635. [[CrossRef](#)]
29. Johir, M.A.H.; Pradhan, M.; Loganathan, P.; Kandasamy, J.; Vigneswaran, S. Phosphate adsorption from wastewater using zirconium (IV) hydroxide: Kinetics, thermodynamics and membrane filtration adsorption hybrid system studies. *J. Environ. Manag.* **2016**, *167*, 167–174. [[CrossRef](#)]

30. Fadhel, A.A.; Johnson, M.; Trieu, K.; Koculi, E.; Campiglia, A.D. Selective nano-sensing approach for the determination of inorganic phosphate in human urine samples. *Talanta* **2017**, *164*, 209–215. [[CrossRef](#)]
31. Song, X.Y.; Ma, Y.; Ge, X.; Zhou, H.J.; Wang, G.Z.; Zhang, H.M.; Tang, X.X.; Zhang, Y.X. Europium-based infinite coordination polymer nanospheres as an effective fluorescence probe for phosphate sensing. *RSC Adv.* **2017**, *7*, 8661–8669. [[CrossRef](#)]
32. Ma, Y.; Zhang, Y.Q.; Li, X.Y.; Yang, P.; Yue, J.Y.; Jiang, Y.; Tang, B. Linker-eliminated nano metal–organic framework fluorescent probe for highly selective and sensitive phosphate ratiometric detection in water and body fluids. *Anal. Chem.* **2020**, *92*, 3722–3727. [[CrossRef](#)] [[PubMed](#)]
33. Salem, J.K.; Draz, M.A. Selective colorimetric nano-sensing solution for the determination of phosphate ion in drinking water samples. *Int. J. Environ. Anal. Chem.* **2020**, *101*, 2329–2338. [[CrossRef](#)]
34. Liu, W.Q.; Du, Z.F.; Qian, Y.; Li, F. A specific colorimetric probe for phosphate detection based on anti-aggregation of gold nanoparticles. *Sens. Actuat. B Chem.* **2013**, *176*, 927–931. [[CrossRef](#)]
35. Pourreza, N.; Sharifi, H.; Golmohammadi, H. A green chemosensor for colorimetric determination of phosphate ion in soil, bone and water samples using curcumin nanoparticles. *Anal. Sci.* **2020**, *36*, 1297–1302. [[CrossRef](#)]
36. GB5009.87-2016; National Food Safety Standard Determination of Food Phosphate. China Food and Drug Administration: Beijing, China, 2008.